PAPER

A novel Li₂FeSiO₄/C composite: Synthesis, characterization and high storage capacity†

Dongping Lv,[a] Wen Wen,[b] Xingkang Huang,[a] Jingyu Bai,[a] Jinxiao Mi,[c] Shunqing Wu[d] and Yong Yang*[a]

A Li₂FeSiO₄/C composite material has been prepared *via* a solution-polymerization approach. The composite is characterized by X-ray diffraction (XRD), X-ray absorption near edge structure (XANES), scanning electron microscope (SEM), transmission electron microscopy (TEM), Fourier transform infrared spectroscopy (FTIR), and superconducting quantum interference device (SQUID). The electrochemical performance of the Li₂FeSiO₄ is greatly enhanced and the initial discharge capacity is ~220 mA h g⁻¹, when it is cycled between 1.5–4.8 V. This indicates that more than one lithium ion can be extracted out of the Li₂FeSiO₄ lattice. At high current densities, the Li₂FeSiO₄/C also exhibits excellent rate capability and cycling stability. This indicates that it is a very promising cathode material for next generation lithium-ion batteries.

Introduction

Rechargeable Li-ion batteries with high-energy density and more environmental benignity are in great demand, especially with the emergence of electric vehicles and the necessary suppression of the CO₂ release, which is very critical for the prevention of global warming.[1] Thus, novel electrode materials with high capacity are widely being explored. Orthosilicate Li₂MSiO₄ (M = Fe, Mn, *etc.*) is a new class of polyanion materials.[2] Besides the high safety arising from the strong Si–O covalent bond, and environmental benignancy and low cost from the characteristics of Fe, Mn, and Si elements, Li₂MSiO₄ may theoretically allow two-electron exchange per formula unit to meet the high-energy density demands.[3] Therefore, Li₂MSiO₄ materials have been investigated intensively in the past few years.[4–18] Among these materials, Li₂FeSiO₄ is attractive as it not only displays outstanding electrochemical behavior,[4,5,14] but it is also the basis for the explosion of substituted derivatives with improved properties.[6,19,20]

However, Li₂FeSiO₄ has low electronic and ionic conductivity.[19] Carbon coating is an efficient way to reduce the particle size and enhance the charge transfer.[21,22] Usually, carbon coating was carried out by mixing Li₂FeSiO₄ or its precursor with a carbon source followed by calcination at high temperature[4,14] and one lithium extraction was realized by charging Li₂FeSiO₄ to 3.8 V as reported by Nyten *et al.*[4] These carbon coating methods, however, may suffer from incomplete coating and inevitable crystal growth at high temperature[23] and to date no more than one lithium ion extraction has been reported on Li₂FeSiO₄.

In this study, a novel Li₂FeSiO₄/C composite was synthesized, where Li₂FeSiO₄ was imbedded into the interconnected carbon frameworks, *via* an *in situ* carbon coating process. This resulted in enhanced electronic conductivity and nanosized particles of the composite, which contributed to more than one lithium ion extraction and excellent rate capability for the composite.

Experimental

Synthesis of the Li₂FeSiO₄/C composite

All chemicals used in our experiments were of analytical grade and used without further purification. The Li₂FeSiO₄/C composite was synthesized *via* a one-step solution-polymerization approach, *i.e.*, no further carbon coating procedure was needed in the process. Fig. S1† shows the schematic flow chart of the synthesis process. Typically, 0.01 mol Fe powder and 0.02 mol citric acid were mixed firstly in 30 mL deionized water under vigorous magnetic stirring at 60 °C, resulting in a white precipitation with release of H₂. The resulting precipitation was dissolved gradually to form a clean jade-green ferrous citrate solution 10 h later. Then stoichiometric amounts of tetraethyl orthosilicate (TEOS) (0.01 mol) and lithium acetate (0.02 mol) were added into the solution and stirred at 60 °C for 4 h, and the solution was still maintained to be transparent. Then 0.01 mol ethylene glycol was added into the solution and the oil bath

[a] State Key Laboratory for Physical Chemistry of Solid Surfaces, College of Chemistry and Chemical Engineering, Department of Chemistry, Xiamen University, Xiamen, 361005, P. R.China. E-mail: yyang@xmu.edu.cn; Tel: +86-592-218-5753
[b] Shanghai Synchrotron Radiation Facility, Shanghai Institute of Applied Physics, Chinese Academy of Science, Shanghai, 201204, China
[c] Department of Materials Science and Engineering, College of Materials, Xiamen University, China
[d] Department of Physics and Institute of Theoretical Physics and Astrophysics, Xiamen University, China
† Electronic supplementary information (ESI) available. See DOI: 10.1039/c0jm03928d

9506 | *J. Mater. Chem.*, 2011, **21**, 9506–9512

This journal is © The Royal Society of Chemistry 2011

temperature was increased to 130 °C and kept for 4 h for polymerization, yielding a viscous transparent polymer precursor. After drying at 80 °C under vacuum for 24 h, the precursor was ground into a powder, pressed into pellets, and subsequently calcined in an Ar atmosphere under a pre-programmed heating process, *i.e.* the temperature was firstly increased to 400 °C at a rate of 2 °C min^{-1} and maintained for 5 h for the complete decomposition of organic groups, and then raised to 600 °C at the same speed and maintained for 10 h for the phase formation of Li_2FeSiO_4.

Preparation of the electrode and electrochemical measurements

The electrochemical cell used in our study was a CR2025 coin cell (Li/electrolyte/cathode) prepared according to our previous work.[24] Firstly, Li_2FeSiO_4/C composite was mixed with acetylene black and poly (vinylidene fluoride) (PVDF) binder with a weight ratio 85 : 5 : 10 (*i.e.*, the content of Li_2FeSiO_4/C in electrode is 85%), and then ground by ball milling at a speed of 500 r min^{-1} for 4 h using N-methyl-2-pyrolidene (NMP) as the solvent. Then the mixture was pressed on aluminum foil (current collector) and thereafter dried under vacuum at 50 °C for 3 h to obtain the cathode. Finally the coin cells were assembled in a dry and inert glove box with the prepared cathode, lithium anode, and Celgard 2400 polypropylene separator. The electrolyte used in our experiment is 1 M $LiPF_6$ in ethylene carbonate/dimethyl carbonate (1 : 1 v/v) solvents. The electrochemical performance was measured galvanostatically at various current densities in a voltage range of 1.5–4.8 V at 30 °C on a LAND CT-2001A (Wuhan, China) battery test system. The charge/discharge specific capacities mentioned in this paper were calculated on the mass of Li_2FeSiO_4 by excluding the carbon content.

Characterization

The structure of the sample was characterized by synchrotron radiation X-ray diffraction (XRD) using BL14B1 at the Shanghai Synchrotron Radiation Facility (SSRF) (Shanghai, China) and the wavelength of X-rays employed is 1.2398 Å. BL14B1 is a bending magnet beamline and the storage ring energy of SSRF is 3.5 GeV. The beam is first collimated using a Rh/Si mirror and then is monochromatized using a Si(1 1 1) double crystal monochromator. After that, the beam is further focused by a Rh/Si mirror to the size of 0.5 mm × 0.5 mm. Higher order harmonics are also rejected by the Rh/Si mirror. NaI scintillation detector was used for data collection.

The *ex-situ* XANES studies were performed at BL14W1 of SSRF and a Si (1 1 1) double crystal monochromator, cooled by liquid nitrogen, was employed to monochromatize the energy. The measurements were performed using transmission mode. The XANES data were analyzed using the Athena program of IFEFFIT for background removal, E_0 selection and normalization, *etc.*[25]

The morphology of the sample was studied using a LEO1530 field emission scanning electron microscope (SEM), equipped with an energy-dispersive X-ray (EDX) detector, and operated at an accelerating voltage of 20 kV. The elemental mapping was done by EDX using area scan mode. The transmission electron microscopy (TEM) and high resolution transmission electron microscopy (HRTEM) were carried out on TECNAI-F30 (Philip-FEI) at an accelerating voltage of 300 kV. The HRTEM images were analyzed using the Gatan micrograph program.

The carbon content in the composite was determined by Vario EL III elemental analyzer (Elementar Analysen System GmbH, Germany). The Fourier transformed infrared spectroscopy (FTIR) was performed on a Nicolet Avatar 360 FTIR (Thermo electro. USA). The magnetization was measured using a superconducting quantum interference device (SQUID) magnetometer (Quantum Design MPMS). *Ex-situ* Mössbauer measurements, on electrodes charged to various voltages, were carried out at room temperature using a Mössbauer spectrometer (Wissel, Germany) working with a constant acceleration mode with a ^{57}Co (Pb) source. The spectra were collected in transmission geometry, and the velocity and isomer shifts were calibrated for a-Fe foil.

Results and discussion

Nanostructured Li_2FeSiO_4/C composite

To enhance electronic conductivity of the materials, our strategy is chelating Li, Fe, and Si ions in a carbon based polymer, which is then calcined to form a Li_2FeSiO_4/C composite. This composite has a nanosized structure, where Li_2FeSiO_4 is embedded in an interconnected carbon framework. To realize this design, it is crucial to construct a polymeric matrix, where all ions are distributed uniformly at the atomic level during the synthesis process. Citric acid was selected as the chelating agent because it has (1) moderate acidity to react with Fe (2) strong chelating ability for various cations[26] (3) a long carbon chain to form a carbon framework. After the reaction of citric acid and Fe (60 °C, 10 h), a transparent solution was obtained successfully and no precipitation resulted by adding TEOS or lithium acetate. The subsequent polymerization was induced by adding ethylene glycol at 130 °C, yielding a jade-green gel, where ethylene glycol acted as a cross-linking agent and bridged all the citric acid complex units together as shown in Fig. S1†. On evaporation, the gel turned into a transparent xerogel without impurity particles inside, which is stable after air exposure. The precalcination temperature of the precursor was 400 °C and the calcination temperature was 600 °C. The selected temperatures were evaluated by thermal analysis (Fig. S2†).

The Fe K-edge XANES spectra of Li_2FeSiO_4 and several reference compounds are displayed in Fig. 1. It can be observed that the Fe K-edge positions shifts to higher energy with the increase of the oxidation state. For Li_2FeSiO_4, the XANES spectrum has an absorption edge around 7120 eV, which has a profile aligning with that of FeO. This indicates that the Fe cation in Li_2FeSiO_4 has a similar valence to that of FeO. However, the spectrum after 7122 eV aligns well with that of the Fe_2O_3, demonstrating that the Li_2FeSiO_4 might have been partially oxidized to $LiFeSiO_4$ due to air exposure during the measurement.[27] The observed weak pre-edge peak in the Li_2FeSiO_4 (Fig. 1 inset) means the tetrahedral coordination of Fe ions in the crystal,[28] which is consistent with the reported result of Dominko *et al.*[29]

SEM images of the Li_2FeSiO_4/C composite are shown in Fig. 2a and b. The particles are micron sized with irregular
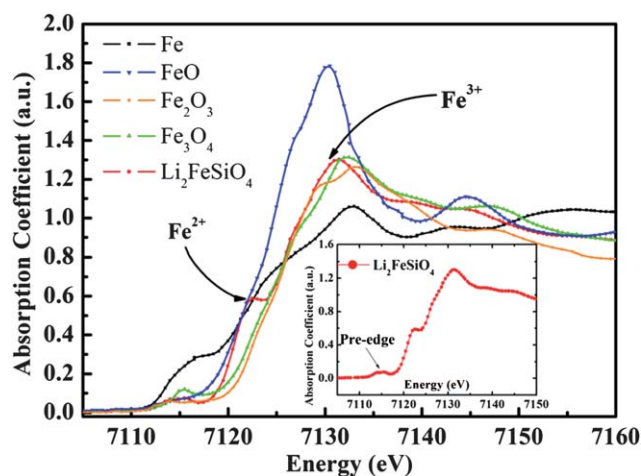
Fig. 1 XANES spectra of Fe, FeO, Fe_2O_3, Fe_3O_4 and Li_2FeSiO_4.

shapes, which may be attributed to interconnection from the carbon frameworks formed during the heat treatment. However, at higher magnification (Fig. 2b), it is found that the large particles consist of smaller nanosized ones of 40–50 nm, with spherical shape and uniform size distribution. The TEM image (Fig. 2d) indicates that Li_2FeSiO_4 particles are in the size of 30–50 nm and connected tightly by carbon. The HRTEM image indicates that Li_2FeSiO_4 is very crystalline and coated by an

amorphous carbon layer (Fig. 2e and f). The EDX (energy dispersive X-ray) of the Li_2FeSiO_4/C composite is displayed in Fig. 2c. It can be observed that Li_2FeSiO_4 particles distribute uniformly in the carbon frameworks, which is consistent with the TEM observation. The carbon content in the Li_2FeSiO_4/C composite is 16%, which is much higher than that of the
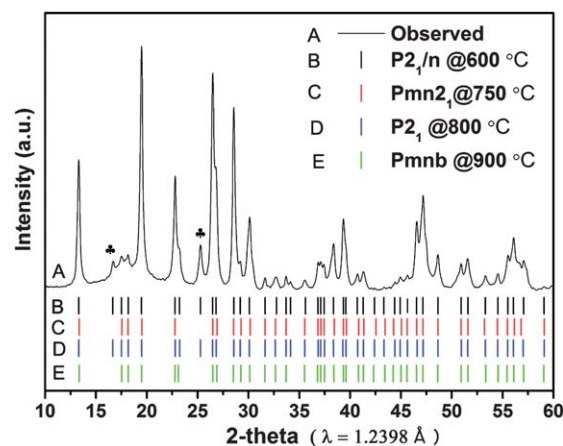

Fig. 3 Synchrotron XRD pattern of Li_2FeSiO_4/C (A). Bragg positions calculated from space groups of $P2_1/n$ (B), $Pmn2_1$ (C), $P2_1$ (D), and $Pmnb$ (E).
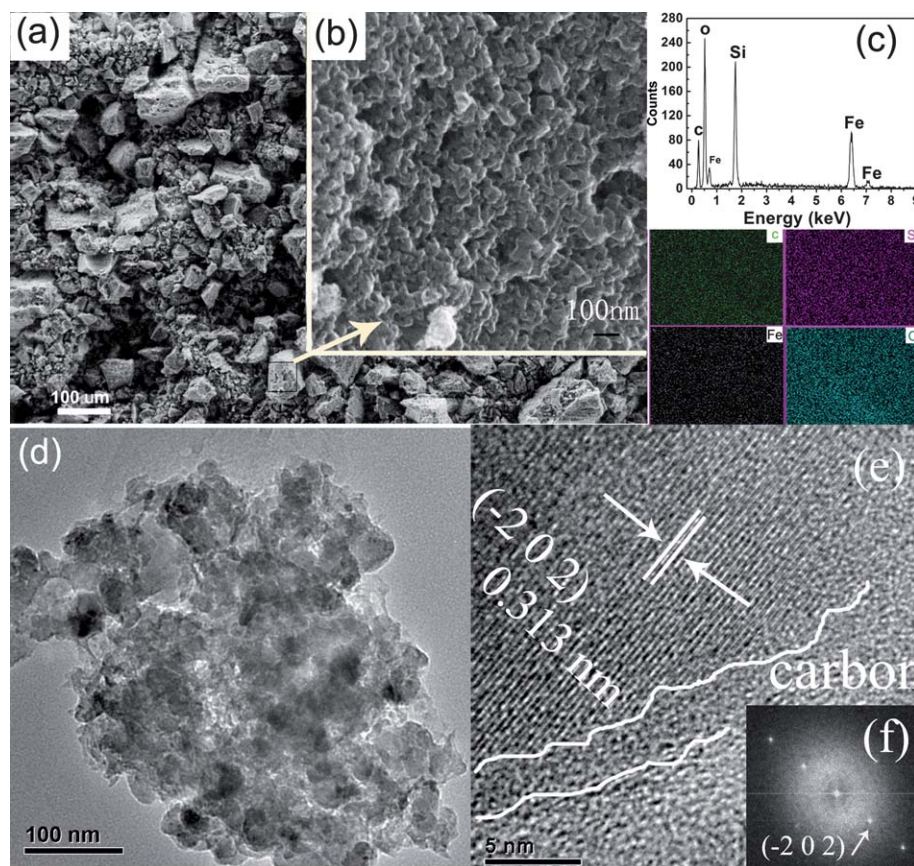

Fig. 2 (a) SEM image of Li_2FeSiO_4/C, (b) magnification of a particle, (c) the EDX result and elemental C, Si, Fe, and O maps, (d) TEM, (e) HRTEM and (f) its corresponding FT image.

LiFePO$_4$/C composite.[21] This might enhance the electrochemical performance, especially at high current densities.

The XRD pattern of Li$_2$FeSiO$_4$ is displayed in Fig. 3, which is consistent with the literature.[4,15,30] It is noted that there are some differences regarding the structure of Li$_2$FeSiO$_4$ in the reported literature. Three kinds of structures are proposed, one is an orthorhombic structure (S.G. *Pmn2$_1$*) with lattice parameters of $a = 6.2661$ Å, $b = 5.3295$ Å, and $c = 5.0148$ Å (C in Fig. 3),[4] another one is an monoclinic structure (S.G. *P2$_1$*) with the lattice parameters of $a = 8.22898$ Å, $b = 5.02002$ Å, $c = 8.23335$ Å and $b = 99.2027°$ (D in Fig. 3),[15] and the third one is also an orthorhombic structure (S.G. *Pmnb*) with lattice parameters of $a = 6.2836$ Å, $b = 10.6572$ Å, and $c = 5.0386$ Å (E in Fig. 3).[31] The main differences among these three models are the orientation of the tetrahedrons (FeO$_4$ and SiO$_4$) and/or whether a super cell is adopted. However, these structures are not a perfect fit for our result. For comparison, Bragg positions calculated according to above three models are displayed in Fig. 3, and it can be observed that for the *Pmn2$_1$* and *Pmnb* models, two diffraction peaks marked by asterisks can not be successfully assigned. Through the combined analysis of high-resolution synchrotron XRD and TEM, Nishimura *et al.* believed that the unidentified diffraction peaks in *Pmn2$_1$* model should be indexed as h/2 k/2 l and consequently a larger symmetric unit with space group *P2$_1$* should be adopted.[15] For our Li$_2$FeSiO$_4$, synthesized at 600 °C coupled with an *in situ* carbon coating, we currently believe that a monoclinic structure with space group *P2$_1$/n* might be a better structural model, which is consistent with the structure of Li$_2$FeSiO$_4$ obtained at 700 °C.[30] Using this model the unidentified diffraction peaks in space groups *Pmn2$_1$* and *Pmnb* could be indexed successfully as displayed in Fig. 3.

The refinement was done assuming a space group of *P2$_1$/n* (Fig. 4), and the refined lattice parameters are $a = 8.2349$ Å, $b = 5.0234$ Å, $c = 8.2436$ Å and $\beta = 99.150°$ with R values of Rp = 6.04% and Rwp = 7.62%. From the refinement result, we can find that the *P2$_1$/n* structure is in fact a superstructure of the unit cell used by Nyten *et al.*[4] Compared to the model *P2$_1$* used by Nishimura *et al.*,[15] it can be found that the *P2$_1$/n* structure has a similar unit cell and the same orientation of the tetrahedrons

(FeO$_4$ and SiO$_4$) (Fig. 4 inset) as that of *P2$_1$*. It is noted that the synthetic method and especially the calcination temperatures have a profound effect on the cation disorder and structural defects in the crystallization process. As a result, the Li$_2$FeSiO$_4$ synthesized at various temperatures and/or *via* different methods always shows the polymorphism and complexity of the crystal structure. For example, Boulineau *et al.* have done a systematic investigation into the temperature effects (700–900 °C) on the polymorphs of Li$_2$FeSiO$_4$ and found a structural evolutional trend from *P2$_1$/n* to *Pmnb* with an increase of temperature.[30] Combining our research at 600 °C, we can find that Li$_2$FeSiO$_4$ prefers *P2$_1$/n* symmetry under temperatures below 700 °C. Although the sample quenched from 900 °C has a symmetry of *P2$_1$/n* ($a = 6.2819$, $b = 10.6575$, $c = 5.0371$ Å and $\beta = 90.032°$),[31] that structure is different to the *P2$_1$/n* which was used in the present work for the sample synthesized at 600 °C ($a = 8.2349$, $b = 5.0234$, $c = 8.2436$ Å and $\beta = 99.150°$). Because there are some differences in lattice parameters for these two structures.

The phase purity of the Li$_2$FeSiO$_4$/C composite was further confirmed by FTIR and magnetic techniques. The FTIR result shows a strong absorbance at 900–930 cm^{-1} (Fig. 5a), which is ascribed to the vibration of SiO$_4^{4-}$.[32] The characteristic absorption peaks of Si–O–Si from Li$_2$SiO$_3$ at 1100 and 780 cm^{-1} are not observed,[33] confirming the absence of Li$_2$SiO$_3$. Fig. 5b is the magnetization curve M(H), where only a linear curve is observed in full range of the magnetic field. Thus, the existence of magnetic phase impurities in the product, such as Fe$_2$O$_3$, is excluded. Combining the results of synchrotron XRD, FTIR, and magnetic experiments, it is concluded that Li$_2$FeSiO$_4$ with high phase purity was synthesized by the solution-polymerization approach.

Electrochemical properties of the Li$_2$FeSiO$_4$/C composite

The initial three cycling profiles of Li$_2$FeSiO$_4$/C (at a current density of 10 mA g^{-1}) are shown in Fig. 6. The 1st discharge capacity of 225 mA h g^{-1}, corresponding to 1.36 mol Li$^+$, is obtained in the initial cycle, which suggests that more than one Li$^+$ can be extracted from the Li$_2$FeSiO$_4$/C. In the literature, it
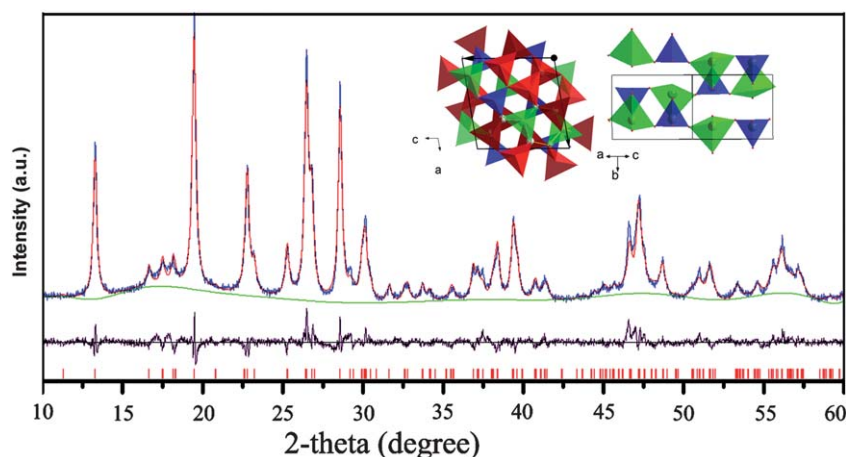
Fig. 4 The XRD pattern of Li$_2$FeSiO$_4$/C and refinement in the space group *P2$_1$/n* (Blue line, experimental; red line, calculation; green line, background; black line, residual). Inset shows representation of the crystal structure of Li$_2$FeSiO$_4$ in the *P2$_1$/n* space group and the tetrahedral arrangement of FeO$_4$ and SiO$_4$. FeO$_4$ (green), SiO$_4$ (blue) and LiO$_4$ (red).

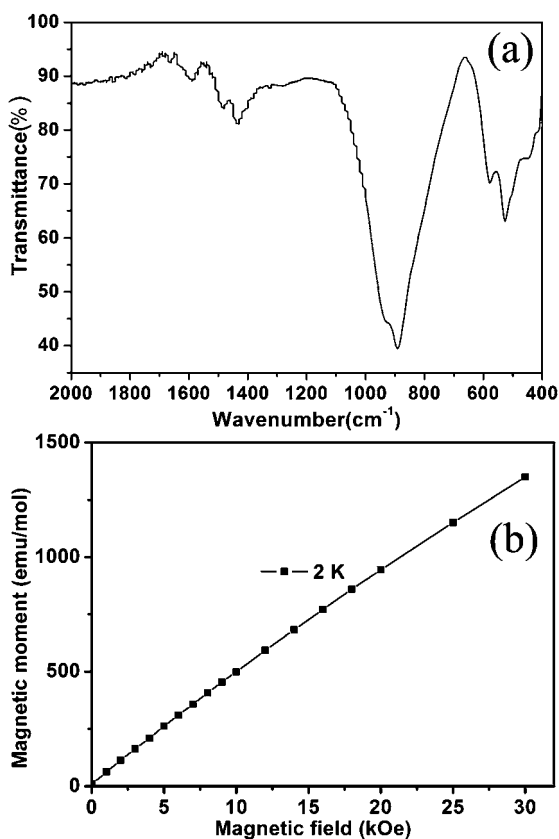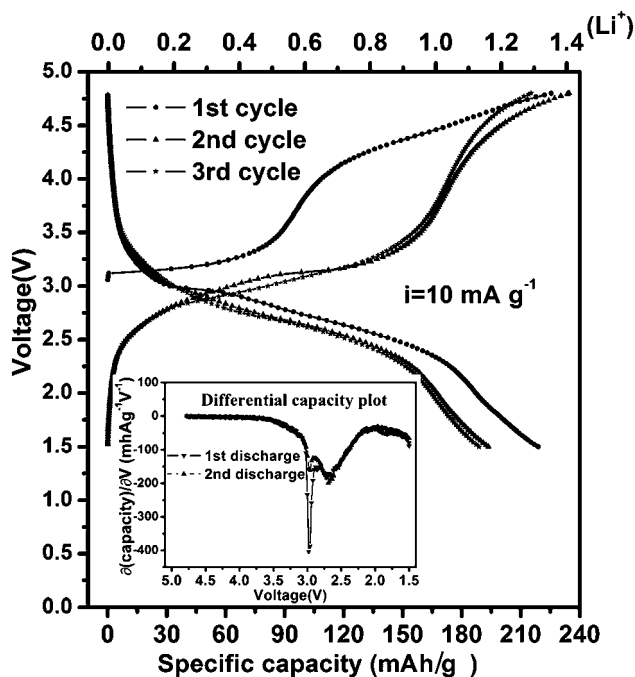**Fig. 5** (a) FTIR spectrum of Li_2FeSiO_4/C, and (b) magnetization as a function of the applied field.

Fig. 6 The charge/discharge curves of the initial three cycles of Li_2FeSiO_4/C at a current density of 10 mA g^{-1} in a voltage range 1.5–4.8 V. Inset shows differential capacity plots of the first and second discharge processes.

was reported that one Li$^+$ can be extracted from Li_2FeSiO_4[4] and further Li$^+$ extraction was difficult due to the poor conductivities of Li_2FeSiO_4.[3] In this work, the new synthetic route ensured a uniform particle size of 30–50 nm and Li_2FeSiO_4 is embedded in a carbon matrix. This greatly enhances the conductivity and helps to extract/insert the second Li$^+$.

Two potential plateaus, located around 3.2 V and 4.3 V, are observed in the initial charge process (Fig. 6). The charge capacities of these two voltage regions are 95 and 135 mA h g^{-1}, respectively. However, in the following charge processes, the charge capacity at 3.2 V region increases to 168 mA h g^{-1}, while that at 4.3 V decreases to 70 mA h g^{-1}.

To clarify the further lithium extraction above the voltage of 4.0 V, the initial charge/discharge performances of Li_2FeSiO_4 in the two voltage ranges (current density of 10 mA g^{-1}) were tested as shown in Fig. 7. When charged to 4.0 V, Li_2FeSiO_4 delivers a discharge capacity of 135 mA h g^{-1}, much lower than that charged to 4.6 V (180 mA h g^{-1}), indicating the further Li$^+$ extraction at higher voltage. It is also found that with the cutoff potential of 4.0 V, the discharge capacity (135 mA h g^{-1}) is larger than the charge capacity (95 mA h g^{-1}). This may be caused by partial oxidation of Li_2FeSiO_4 to $LiFeSiO_4$ during the electrode preparation.[27]

To study the possibility that the Li$^+$ extraction above 4.0 V may relate to further oxidation of Fe^{3+} to Fe^{4+}, *ex-situ* Mössbauer measurements were carried out on the electrodes charged to various potentials as shown in Fig. 8. According to the fitting parameters summarized in Table 1, the Li_2FeSiO_4 electrode is partially oxidized to $LiFeSiO_4$ (35.7%) before the electrochemical test. That is confirmed by the coexistence of two doublets with isomer shift (I.S.) values of +0.26 and +1.02 mm s^{-1}, which are ascribed to tetrahedral Fe^{3+} and Fe^{2+}, respectively.[7,34] In the charging process up to 3.8 V, the remained Li_2FeSiO_4 (64.3%) is transformed to $LiFeSiO_4$ upon Li$^+$ extraction with a charge capacity of *ca.* 100 mA h g^{-1} (Fig. 6). When the electrode is charged to 4.2 V, a new doublet with a decreased I.S. value of 0.14 mm s^{-1} is observed, indicating the transformation
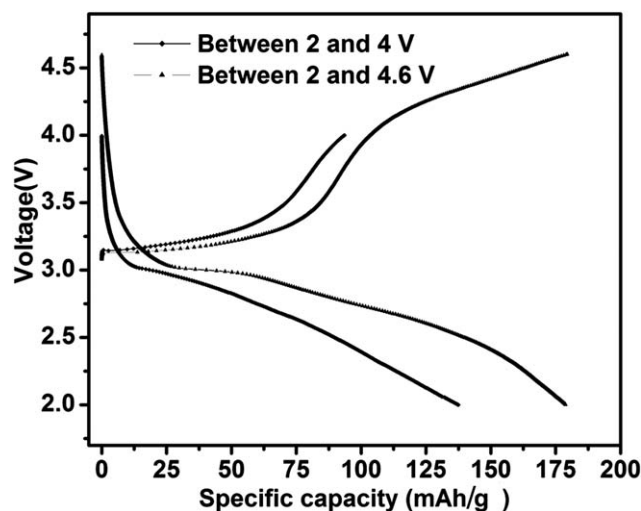

Fig. 7 Comparison of charge/discharge curves in the initial cycles between the voltage ranges 2.0–4.6 V and 2.0–4.0 V at a current density of 10 mA g^{-1}.
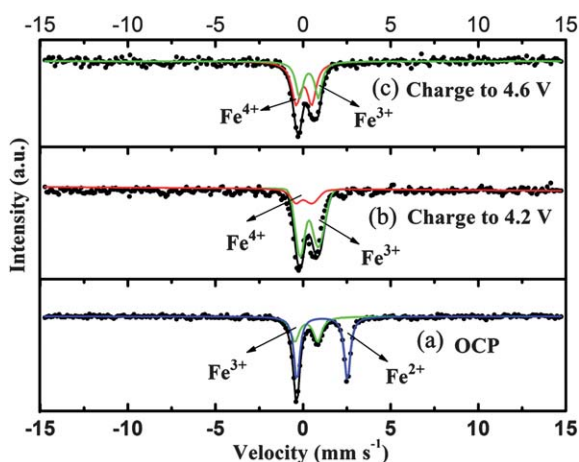
Fig. 8 Mössbauer spectra of Li$_2$FeSiO$_4$/C electrodes at (a) OCP (open circuit potential), (b) charge to 4.2 V and (c) charge to 4.6 V.

Table 1 Mössbauer parameters fitting results for Li$_2$FeSiO$_4$ electrodes charged to various potentials

Sample	Component	I.S. (mm s^{-1})	Q.S. (mm s^{-1})	Area (%)
OCP	Fe^{2+}	1.02(1)	2.42(1)	64.3
	Fe^{3+}	0.26(2)	1.09(2)	35.7
4.2 V	Fe^{3+}	0.38(2)	0.83(1)	79.3
	Fe^{4+}	0.14(2)	0.72(2)	20.7
4.6 V	Fe^{3+}	0.39(2)	0.90(2)	41.8
	Fe^{4+}	0.13(2)	0.75(2)	58.2

of LiFeSiO$_4$ to FeSiO$_4$ with the formation of Fe^{4+}.[34,35] Charged to a higher potential of 4.6 V, the doublet area of Fe^{4+} increases from 20.7% (at 4.2 V) to 58.2%, suggesting the further oxidation of Fe^{3+}. It should be mentioned that the quantitative analysis of the doublet area change does not match strictly with the evolution of charge/discharge capacity, which may be caused by the relatively low signal to noise ratio of the Mössbauer spectra.

The cycling performance of Li$_2$FeSiO$_4$/C at 10 mA g^{-1} between 1.5 and 4.8 V is shown in Fig. 9a. Compared to the initial discharge process, there is a capacity decay of 20 mA h g^{-1} in the second discharge process. On the analysis of differential capacity plots of the first and second discharge processes (Fig. 6, inset), it is clear that the capacity decay is mainly caused by the disappearance of discharge plateau at 3.0 V in the second discharge process. In the following cycles, relatively stable cycling performance is observed. For example, *ca.* 190 and 170 mA h g^{-1} are obtained for the 10th and 30th cycles, respectively. Compared to the excellent cycling stability of Li$_2$FeSiO$_4$ upon less than one lithium ion extraction,[4,14,36] we attribute the slow capacity decay in our product to gradual structural rearrangements when more than one mole of Li$^+$ is extracted from Li$_2$FeSiO$_4$. In addition, it should also be taken into account that the side reactions from the electrolyte at high potential is inevitable and detrimental to the cycling stability.[37]

The rate capability as well as the cycling stability of the composite was further investigated by changing the cycling rates repeatedly (Fig. 9b). In the prolonged cycling of Li$_2$FeSiO$_4$/C, a discharge capacity of *ca.* 135 mAh g^{-1} is obtained at

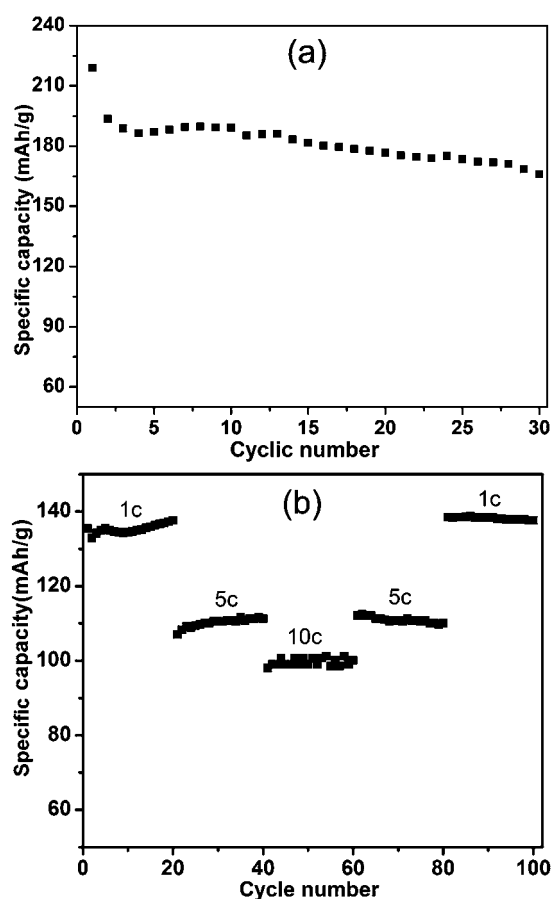**Fig. 9** (a) Cycling performance of Li$_2$FeSiO$_4$/C at a current density of 10 mA g^{-1} and (b) rate performances of Li$_2$FeSiO$_4$/C at various repeated current densities.

1C (1C = 166 mA g^{-1}) rate; and *ca.* 100 mA h g^{-1}, 75% of that at 1 C, is obtained even at 10 C rate, suggesting the good rate capability of the Li$_2$FeSiO$_4$/C. In repeated cycling processes, the discharge capacities can be repeated along the variation of rates, indicating the fine stability at high rates when less than one Li$^+$ per Li$_2$FeSiO$_4$ formula unit is extracted reversibly. We attribute the excellent performance of this material, *i.e.*, high capacity with exceeding one Li$^+$ extraction in Li$_2$FeSiO$_4$ and high rate capability, to the novel Li$_2$FeSiO$_4$/C structure, where nanosized Li$_2$FeSiO$_4$ particles are embedded within the interconnected carbon frameworks. Such a structure benefits the high capacity when such a phase pure product is charged to a high voltage of 4.8 V, fast kinetics of Li$^+$ insertion/extraction from nanosized particles,[38] and fast electron transfer along the interconnected carbon framework.[39–41]

Conclusions

Novel Li$_2$FeSiO$_4$/C composite was successfully synthesized *via* a solution-polymerization approach. The Li$_2$FeSiO$_4$ synthesized at 600 °C has high phase purity and a monoclinic structure with the space group *P*2$_1$/*n*. The *in situ* formed interconnected carbon framework enabled the complete and immediate carbon coating and suppressed the crystal growth at high temperature. This greatly enhanced the electron transfer and Li$^+$ kinetics in the electrochemical process.

Cycled between 4.8 and 1.5 V (*e.g.*, 10 mA g^{-1}) at 30 °C, more than one Li$^+$ can be extracted/inserted (*e.g.*, 1.3 mol per formula unit) out/into the Li$_2$FeSiO$_4$ lattice. During the charge process, two plateaus, located at 3.2 V and 4.3 V, were observed in the voltage range 3–4.8 V, which were related to the two lithium extraction reactions. The first lithium was fully extracted at 3.2 V, with the oxidation of Fe^{2+} to Fe^{3+}. The second lithium was partially extracted at 4.3 V. Furthermore, the Li$_2$FeSiO$_4$/C composite displayed a much improved rate capability. For example, 135 mA h g^{-1} and 100 mA h g^{-1} were obtained at 1C and 10 C rates, respectively. These results indicated the novel Li$_2$FeSiO$_4$/C composite is a promising candidate as a cathode material for Li-ion batteries.

Acknowledgements

References

1 J. M. Tarascon and M. Armand, *Nature*, 2001, **414**, 359.
2 M. Armand, World Patent, WO02/27823, 2002.
3 M. E. Arroyo-de Dompablo, M. Armand, J. M. Tarascon and U. Amador, *Electrochem. Commun.*, 2006, **8**, 1292.
4 A. Nyten, A. Abouimrane, M. Armand, T. Gustafsson and J. O. Thomas, *Electrochem. Commun.*, 2005, **7**, 156.
5 R. Dominko, M. Bele, M. Gaberscek, A. Meden, M. Remskar and J. Jamnik, *Electrochem. Commun.*, 2006, **8**, 217.
6 Z. L. Gong, Y. X. Li and Y. Yang, *Electrochem. Solid-State Lett.*, 2006, **9**, A542.
7 A. Nyten, S. Kamali, L. Haggstrom, T. Gustafsson and J. O. Thomas, *J. Mater. Chem.*, 2006, **16**, 2266.
8 A. S. Prakash, P. Rozier, L. Dupont, H. Vezin, F. Sauvage and J. M. Tarascon, *Chem. Mater.*, 2006, **18**, 407.
9 K. Zaghib, A. A. Salah, N. Ravet, A. Mauger, F. Gendron and C. M. Julien, *J. Power Sources*, 2006, **160**, 1381.
10 R. Dominko, M. Bele, A. Kokalj, M. Gaberscek and J. Jamnik, *J. Power Sources*, 2007, **174**, 457.
11 Z. L. Gong, Y. X. Li and Y. Yang, *J. Power Sources*, 2007, **174**, 524.
12 Y. X. Li, Z. L. Gong and Y. Yang, *J. Power Sources*, 2007, **174**, 528.
13 C. Lyness, B. Delobel, A. R. Armstrong and P. G. Bruce, *Chem. Commun.*, 2007, 4890.
14 Z. L. Gong, Y. X. Li, G. N. He, J. Li and Y. Yang, *Electrochem. Solid-State Lett.*, 2008, **11**, A60.
15 S. I. Nishimura, S. Hayase, R. Kanno, M. Yashima, N. Nakayama and A. Yamada, *J. Am. Chem. Soc.*, 2008, **130**, 13212.
16 S. Zhang, C. Deng and S. Y. Yang, *Electrochem. Solid-State Lett.*, 2009, **12**, A136.
17 N. Kuganathan and M. S. Islam, *Chem. Mater.*, 2009, **21**, 5196.
18 I. Belharouak, A. Abouimrane and K. Amine, *J. Phys. Chem. C*, 2009, **113**, 20733.
19 A. Kokalj, R. Dominko, G. Mali, A. Meden, M. Gaberscek and J. Jamnik, *Chem. Mater.*, 2007, **19**, 3633.
20 N. Recham, M. Casas-Cabanas, J. Cabana, C. P. Grey, J. C. Jumas, L. Dupont, M. Armand and J. M. Tarascon, *Chem. Mater.*, 2008, **20**, 6798.
21 N. Ravet, M. Simoneau, A. Vallee, M. Armand, Canadian Pattent, 2270771, 1999.
22 A. Yamada, S. C. Chung and K. Hinokuma, *J. Electrochem. Soc.*, 2001, **148**, A224.
23 A. A. Salah, A. Mauger, K. Zaghib, J. B. Goodenough, N. Ravet, M. Gauthier, F. Gendron and C. M. Julien, *J. Electrochem. Soc.*, 2006, **153**, A1692.
24 D. P. Lv, X. K. Huang, H. J. Yue and Y. Yang, *J. Electrochem. Soc.*, 2009, **156**, A911.
25 B. Ravel and M. Newville, *Phys. Scr.*, 2005, **T115**, 1007.
26 W. Liu, K. Kowal and G. C. Farrington, *J. Electrochem. Soc.*, 1998, **145**, 459.
27 A. Nyten, M. Stjerndahl, H. Rensmo, H. Siegbahn, M. Armand, T. Gustafsson, K. Edstrom and J. O. Thomas, *J. Mater. Chem.*, 2006, **16**, 3483.
28 J. Wong, F. W. Lytle, R. P. Messmer and D. H. Maylotte, *Phys. Rev. B*, 1984, **30**, 5596.
29 R. Dominko, I. Arcon, A. Kodre, D. Hanzel and M. Gaberscek, *J. Power Sources*, 2009, **189**, 51.
30 A. Boulineau, C. Sirisopanaporn, R. Dominko, A. R. Armstrong, P. G. Bruce and C. Masquelier, *Dalton Trans.*, 2010, **39**, 6310.
31 C. Sirisopanaporn, A. Boulineau, D. Hanzel, R. Dominko, B. Budic, A. R. Armstrong, P. G. Bruce and C. Masquelier, *Inorg. Chem.*, 2010, **49**, 7446.
32 M. Ganesan, *Ionics*, 2007, **13**, 379.
33 D. Cruz and S. Bulbulian, *J. Am. Ceram. Soc.*, 2005, **88**, 1720.
34 H. Shigemura, H. Sakaebe, H. Kageyama, H. Kobayashi, A. R. West, R. Kanno, S. Morimoto, S. Nasu and M. Tabuchi, *J. Electrochem. Soc.*, 2001, **148**, A730.
35 G. Prado, A. Rougier, L. Fournes and C. Delmas, *J. Electrochem. Soc.*, 2000, **147**, 2880.
36 R. Dominko, D. E. Conte, D. Hanzel, M. Gaberscek and J. Jamnik, *J. Power Sources*, 2008, **178**, 842.
37 P. Arora, R. E. White and M. Doyle, *J. Electrochem. Soc.*, 1998, **145**, 3647.
38 A. S. Arico, P. Bruce, B. Scrosati, J. M. Tarascon and W. Van Schalkwijk, *Nat. Mater.*, 2005, **4**, 366.
39 H. Huang, S. C. Yin, T. Kerr, N. Taylor and L. F. Nazar, *Adv. Mater.*, 2002, **14**, 1525.
40 X. L. Wu, L. Y. Jiang, F. F. Cao, Y. G. Guo and L. J. Wan, *Adv. Mater.*, 2009, **21**, 2710.
41 X. L. Ji, K. T. Lee and L. F. Nazar, *Nat. Mater.*, 2009, **8**, 500.